articulo_upeu_2 (21) (1).pdf

por Ivan SOTO RODRÍGUEZ

Fecha de entrega: 08-jul-2025 07:00p. m. (UTC-0500)
Identificador de la entrega: 2712148561
Nombre del archivo: articulo_upeu_2_21_1_.pdf (2.44M)
Total de palabras: 8773
Total de caracteres: 46277

Journal of Enhanced Heat Transfer, 1(1):1–25 (2025)

PARAMETRIC EVALUATION OF SOLAR CHIMNEY PERFORMANCE THROUGH CFD SIMULATION AND MULTIVARIATE STATISTICAL ANALYSIS USING CHERNOFF FACES

A. Hananel,[1,2,*] *S. Loaiza,*[1,2] *I. Soto,*[1] *R. Garcia,*[2] *& A. Vera*[2]

[1]*Escuela de Posgrado, Universidad Peruana Unión, Lima, Peru, 15464*
[2]*Department of Engineering, Santo Toribio de Mogrovejo Catholic University, Chiclayo, Peru, 14001*

*Address all correspondence to: A. Hananel, Escuela de Posgrado, Universidad Peruana Unión, Lima, Peru, 15464, E-mail: ahananel@upeu.edu.pe

Original Manuscript Submitted: 06/16/2025; Final Draft Received: 06/16/2025

This paper presents an integrated study of computational simulation (CFD) and multivariate statistical analysis aimed at optimizing the design of solar chimneys. The Manzanares plant was taken as a reference model in ANSYS Fluent. Based on the results obtained, eleven regression models were explored to describe the behavior of air velocity as a function of the scale parameter, validating their equations using statistical metrics and multivariate graphical representations. The methodology included the innovative use of Chernoff faces to visually synthesize fifteen statistical variables per model, thus facilitating structured comparison and identification of the most representative model. The power-type regression model was determined to be the most suitable, as it showed the highest degree of fit to the simulated data, theoretical consistency with the modeled physical phenomenon, and a visually favorable expression under different scenarios. Specific equations for different irradiance levels were formulated; in addition, efficiency and generated power were estimated, contrasting the results with previous research. The analysis was enriched by incorporating geometric variables such as the height and radius of the chimney and collector, confirming that scale reduction significantly compromises performance. This visual-statistical approach not only validates CFD-derived models but also introduces an intuitive and effective tool for decision-making in solar engineering. It is concluded that Chernoff faces constitute a methodological strategy applicable to the study of energy performance, opening new lines of research and optimized design through multivariate visualization.

KEY WORDS: *Solar chimneys, CFD, Multivariate statistics, Chernoff faces, nonlinear regression*

1. INTRODUCTION

Statistics is a fundamental research tool that enables the description of phenomena and the development of appropriate problem-solving approaches, based on inferences drawn from data analysis. As Santos and Peña (2017) points out, in the context of higher education, the production of large volumes of data makes the use of rigorous statistical methods indispensable for their processing, analysis, and interpretation.

One of the most innovative contributions to multivariate data representation was proposed by Chernoff (1973), who developed a graphical method based on the use of faces with parameterized facial features. Each facial feature represents a specific quantitative variable, leveraging the human innate ability to identify patterns in faces. His paper entitled *The Use of Faces to Represent Points in k-Dimensional Space Graphically* introduced an intuitive visual technique for exploring high-dimensional data, facilitating the detection of correlations and latent structures. This approach is based on the mathematical analysis of distances, eccentricities, and geometric proportions, making it a powerful tool for interpreting complex data.

The application of this methodology was consolidated in the late 1990s as an exploratory graphical alternative for representing multidimensional data sets. Research such as Flury and Riedwyl (1981) highlighted the usefulness of matrix plots as a form of visual synthesis. However, as Olmos (1997) warned, the lack of specialized software at that time limited the development of research employing multivariate statistical methods, particularly in the context of experimental designs.

In the field of renewable energy engineering, one of the most relevant experimental studies was conducted by Haaf et al. (1983), who documented the construction of a solar plant in Manzanares (Spain) based on the greenhouse effect principle. In this system, air is heated under a collector cover, its density is reduced, and it rises through a central tower, generating a flow that drives turbines coupled to electrical generators. Although a large amount of data was collected in that experiment, Chernoff's methodology could not have been applied due to the technological limitations at that time. Currently, this situation has changed significantly. Studies such as Cuicas Ávila et al. (2007) highlight the importance of using mathematical software in education and research. Nonetheless, as F Medina Martínez (2017) points out, many advances in areas such as statistics are still not fully exploited in engineering research. Even so, simple geometric propositions —for example, considering that a solar chimney is convergent if it has a cylindrical shape and divergent if it has an inlet or outlet angle— demonstrate that geometric variables can be evaluated parametrically using the Chernoff faces method. This allows establishing analogies between the structural features of a solar chimney and the facial attributes of a visage, revealing relevant patterns that might go unnoticed in a conventional analysis (see Figure 1).

Given that the main objective of this research is to carry out a parametric evaluation of solar design variables under the Chernoff methodology, various indicators typically analyzed univariately in regression models derived from CFD (e.g., air velocity, pressure, temperature, mass flow, among others) were examined at a multivariate level. Although numerical simulations allow solving differential equation systems that model airflow in a solar chimney, the resulting equations must be mathematically grounded to be considered valid approximations. Analogous to multivariate statistics, where facial features synthesize multiple dimensions of the data, it is proposed that in solar chimney design its key variables can also be parameterized to optimize the system's performance and energy efficiency.

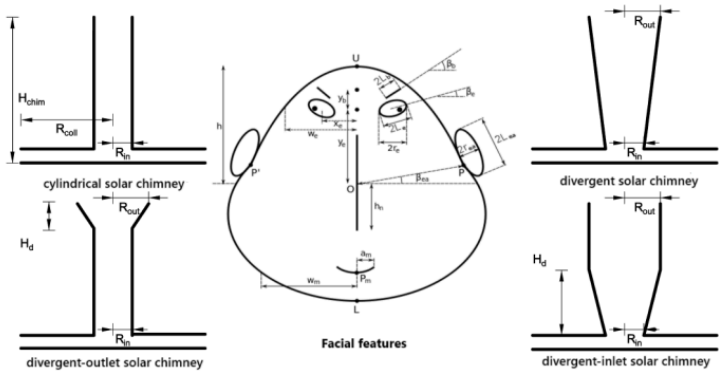

Figure 1: Relationship between perception variables of solar chimney parameters and facial features.

1.1 State of the art

Since the landmark Manzanares experiment, numerous studies have deepened and expanded knowledge about solar chimneys. The results obtained at that plant continue to serve as a fundamental reference to validate current research and advanced numerical simulations in mechanical design. Xu and Zhou (2018) carried out solar chimney simulations in order to evaluate their performance through a parametric analysis of the relationship between the inlet and outlet areas of the tower. Their findings indicated that adjusting these geometric areas can significantly improve the system's energy efficiency, providing a solid basis for the mathematical study of the involved parametric equations.

This approach was supported by Hu et al. (2017), who demonstrated that solar chimneys with different inlet and outlet areas outperform conventional cylindrical configurations, such as the Manzanares design. Their study reported a greater potential in terms of energy generation, mass flow, and electrical output, influenced by key geometric variables such as the area ratio and the height-to-radius ratio of the collector. These results were validated by comparing CFD simulations with experimental data, revealing nonlinear behavior and setting an important precedent for future research on non-cylindrical solar chimneys.

In a complementary manner, Mebarki et al. (2022) conducted a CFD analysis focused on the optimization of solar power plants with chimneys, emphasizing that reducing the scale factor in the geometric model has a direct impact on energy generation. Their study suggests the possibility of implementing these structures in urban areas as a sustainable alternative. Similarly, Murena et al. (2022) established correlations between air velocity and environmental parameters, highlighting the strong dependence of velocity on solar irradiance and temperature. Both studies agree on the need for rigorous theoretical analysis, validated by CFD simulations, to improve the performance of these systems.

In the Peruvian case, the country of origin of the authors of this research, only one relevant experimental precedent has been identified, developed by Velazco Lorenzo and Butler Blacker (2022). That study consisted of the construction of an academic solar-wind chimney model for energy supply in a university facility. Although it was oriented towards photovoltaic energy, the work demonstrated technical feasibility on a small scale; however, it did not incorporate a parametric analysis or an exhaustive mathematical treatment of performance variables.

This gap in the national literature justifies the application of an innovative methodology based on multivariate visualization using Chernoff faces, aimed at complementing existing CFD approaches. In this context, the present research seeks not only to improve solar chimney performance but also to facilitate the understanding of multiple physical variables inherent in Computational Fluid Dynamics, through an accessible visual tool.

Likewise, it is proposed that the optimized design of solar chimneys can become, in the long term, a viable and sustainable alternative in the face of climate change effects. This is particularly relevant for regions such as Lambayeque, where the coexistence of extreme climates significantly affects vulnerable populations. Therefore, this study provides a substantial added value by integrating the statistical and mathematical analysis of equations derived from CFD with a visual and multidisciplinary approach based on the use of Chernoff faces. The decisions made within this methodological framework are not only grounded in numerical evidence but also in the visual interpretation of patterns through facial features, which adds a unique cognitive and exploratory dimension to the analysis and improvement proposals.

1.2 Mathematical model

The behavior of fluid flow can be understood by tracking the displacement of each of its particles as a function of position. However, this approach is often tedious, so an efficient alternative is to study the velocity of the fluid, denoted as $\mathbf{V} = (v_x, v_y, v_z)$, where $\mathbf{V} = \left(\frac{\partial u}{\partial x}, \frac{\partial u}{\partial y}, \frac{\partial u}{\partial z}\right)$. The determination of these velocity components requires solving the differential equation of mass conservation in Cartesian coordinates, where ρ is the density:

$$\frac{\partial \rho}{\partial t} + \frac{\partial \rho v_x}{\partial x} + \frac{\partial \rho v_y}{\partial y} + \frac{\partial \rho v_z}{\partial z} = 0$$

This equation can be expressed more compactly as:

$$\frac{\partial \rho}{\partial t} + \operatorname{div}(\rho \mathbf{V}) = 0$$

Due to the geometry of the solar chimney, it is convenient to transform this equation to cylindrical coordinates (r, θ, z):

$$\frac{\partial \rho}{\partial t} + \frac{1}{r}\frac{\partial (\rho r v_r)}{\partial r} + \frac{1}{r}\frac{\partial (\rho v_\theta)}{\partial \theta} + \frac{\partial (\rho v_z)}{\partial z} = 0$$

where ρ is the fluid density and $\mathbf{v} = (v_r, v_\theta, v_z)$ is the velocity in the cylindrical system, with v_r, v_θ and v_z representing the radial, angular, and vertical components of velocity, respectively. In a solar chimney, it is generally assumed that $v_\theta = 0$. By rearranging, the continuity equation is obtained:

$$\frac{\partial \rho}{\partial t} + \frac{\partial (\rho v_z)}{\partial z} + \frac{1}{r}\frac{\partial (\rho r v_r)}{\partial r} = 0$$

The momentum equation in the radial direction, with μ as the dynamic viscosity and p as the pressure, is:

$$\rho g - \frac{\partial p}{\partial r} + \mu\left(\frac{\partial}{\partial r}\left(\frac{1}{r}\frac{\partial (r v_r)}{\partial r}\right) + \frac{\partial^2 v_r}{\partial z^2} - \frac{v_r}{r^2}\right) = \rho\left(v_r\frac{\partial v_r}{\partial r} + v_z\frac{\partial v_r}{\partial z} + \frac{\partial v_r}{\partial t}\right)$$

The momentum equation in the vertical direction is:

$$\rho g - \frac{\partial p}{\partial z} + \mu \left(\frac{1}{r} \frac{\partial}{\partial r} \left(r \frac{\partial v_z}{\partial r} \right) + \frac{\partial^2 v_z}{\partial z^2} \right) = \rho \left(v_r \frac{\partial v_z}{\partial r} + v_z \frac{\partial v_z}{\partial z} + \frac{\partial v_z}{\partial t} \right)$$

Replacing the components (v_r, v_z) for the calculation of temperature T and considering the radiative heat flux vector q_r in the energy equation, with λ as the thermal conductivity and C_p as the specific heat:

$$\frac{\partial(\rho C_p T)}{\partial t} + \frac{1}{r} \frac{\partial}{\partial r} (\rho r C_p v_r T) + \frac{\partial(\rho C_p v_z T)}{\partial z} = \frac{1}{r} \frac{\partial}{\partial r} \left(r \lambda \frac{\partial T}{\partial r} \right) + \frac{\partial}{\partial z} \left(\lambda \frac{\partial T}{\partial z} \right) - \mathrm{div}(q_r)$$

This equation, along with the continuity equation, can be reformulated in terms of temperature and pressure to compute the total energy per unit mass E:

$$\frac{\partial(\rho E)}{\partial t} + \nabla \cdot (\rho \mathbf{v} E + \mathbf{v} p) = \nabla \cdot (\lambda \nabla T) - \mathrm{div}(q_r)$$

where S represents source terms. In the case of a solar chimney, the parametric research focuses on the vertical component of velocity v_z.

1.3 Classical formulas for the efficiency and performance analysis of a solar chimney

The classic formulas for evaluating the efficiency and performance of a solar chimney are based on the definitions of pressure and volumetric flow rate. Pressure is determined by solving the system of partial differential equations presented in the momentum equation in section 1.2. On the other hand, volumetric flow rate is calculated from the mass flow rate.

Mass flow, denoted by $\dot{m}$, represents the amount of mass transported through a cross-section of the system per unit time. The flow is related to the fluid density (ρ) and the volumetric flow rate (V). The volumetric flow rate is defined as the ratio of the mass flow to the fluid density: $V = \dot{m}/\rho$.

For the power output considering the pressure drop rate in the turbine (χ), the formula used is:

$$P = \eta_{turb} \chi \sqrt{1 - \chi} \Delta p_{poten} V \tag{1}$$

where η_{turb} is the turbine efficiency, χ is the pressure drop rate across the turbine, $\Delta p_{\mathrm{poten}}$ is the potential pressure, and V is the volumetric flow rate.

If the parameter χ is not considered, the power is calculated with the formula:

$$P = \eta_{turb} \Delta p_{turb} V \tag{2}$$

where Δp_{turb} is the static pressure difference across the turbine, and the rest of the parameters are as previously described.

The values necessary for these calculations, extracted from the studies cited in section 1.3, have been used as the basis for this analysis. These data, along with the methodology and results described by the mentioned authors, have been fundamental for evaluating the efficiency and performance of this research, the analysis of which is presented in section 3.

2. METHODOLOGY

Firstly, part of the CFD methodology from the classic study on solar chimneys conducted by Haaf at the Manzanares solar plant, previously mentioned, was replicated. Secondly, a design methodology aimed at improving the performance of a solar chimney was developed, validating CFD-derived mathematical formulas through facial feature analysis. For this purpose, the programs Ansys Fluent, Statistica, and R were used, applied to both the numerical and statistical analysis of the simulations, as well as to the implementation of the corresponding procedures.

2.1 Geometric parameters

The geometric parameters of the solar chimney, expressed in meters, are specified for the height and radius of both the chimney (H_{chim} and R_{chim}) and the collector ($H_{\text{collector}}$ and $r_{\text{collector}}$). These parameters were considered at full scale ($C = 1$) and are detailed in Table 1. These values are fundamental for the accurate modeling of the solar chimney in this study.

Table 1: Values of some geometric parameters of the Manzanares solar chimney plant (adapted from Haaf et al. (1983))

Scale (C)	H_{chim} (m)	R_{chim} (m)	$H_{\text{collector}}$ (m)	$r_{\text{collector}}$ (m)
Full scale (C=1, 1:1)	195	115	27	125

2.2 Modeling and meshing

A three-dimensional model of the Manzanares solar plant in Spain, as defined in Haaf et al. (1983), was implemented. Its cylindrical geometry and a disk-shaped collector were designed in Solidworks and imported into ANSYS Fluent for simulation. There, a tetrahedral mesh was used (see Fig. 2), specifying certain boundary conditions necessary to initiate the simulation, along with other parameters entered in the program such as the density ($\rho = 1.103\,\text{kg/m}^3$) and the ambient pressure (93.9 kPa), respectively.

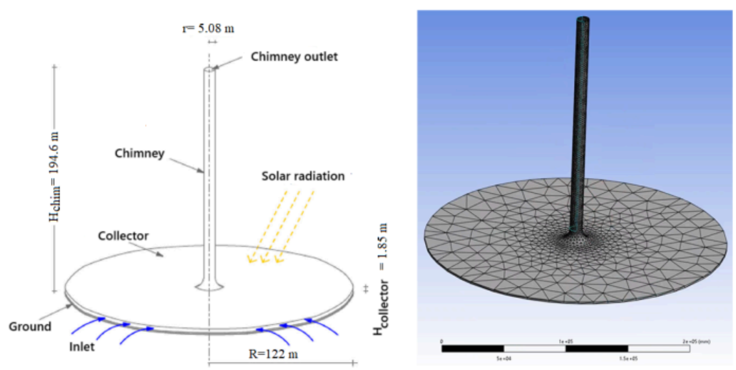

Figure 2: Modeling and meshing applied in the CFD analysis.

2.3 Boundary conditions

The following boundary conditions were set in Ansys Fluent:

- **Wall:**
  - Collector roof: Thermally insulated.
  - Chimney surface: Thermally insulated.
  - Transition section from collector to chimney: Thermally insulated.
  - Ground (effective heat flux = efficiency × irradiance): $0.294 \times 850 = 250$ W/m^2.
- **Inlet:**
  - Collector inlet (no difference from ambient atmosphere).
  - Gauge pressure: 0 Pa.
  - Ambient ground-level temperature: 296.65 K (23.5 °C).
- **Outlet:**
  - Chimney outlet (no difference from ambient atmosphere).
  - Gauge pressure: 0 Pa.
  - Ambient ground-level temperature: 296.65 K (23.5 °C).
- **Ventilation (Turbine):**
  - Pressure drop (Δp_{turb}):
    * For simulated data: None (0 Pa).
    * For actual data (Validation): Non-zero (82.9 Pa).
  - Height at which it is located: 10 m.

2.4 Simulation parameters

After inputting the boundary conditions and performing the first simulation, the Rayleigh number was theoretically calculated using the formula

$$Ra = \frac{b}{a}\, g\, H_{\text{col}}^3 \frac{\Delta T}{v_z},$$

where v_z and ΔT were obtained as the maximum temperature difference from the simulation across the entire system geometry, and b and a are the expansion coefficient and thermal diffusivity, respectively. The resulting Ra was found to be greater than 1000, indicating that the flow was turbulent, a crucial consideration to reformulate the conditions of subsequent simulations.

2.5 Physical-mathematical model underlying the simulation

The foundation of our methodology was based on the mathematical analysis of the parametric evaluation of the theoretical CFD variables. This analysis was structured in the following points, which constitute the pillars of the consistency of our framework:

1. **Parametric formula of the continuity equation:** It is known that hydrostatic pressure is a physical formula that describes the behavior of fluids in equilibrium under gravity, linking it to the fluid density (ρ) and the height (H) in the form $P = \rho g H$. The velocity considered in the model (v_b or v_t) is the velocity in the radial direction (at the base or at the top of the chimney, respectively), i.e. the speed at which a point on the surface of the cylinder is moving toward or away from the central axis (positive if moving outward, negative if moving inward). It is also known from the continuity equation that the volumetric flow rate is constant at any cross-section of the duct. Therefore, $A_1 v_1 = A_2 v_2$. Applied to the solar chimney, $A_t v_t = A_b v_b$, which can be written in terms of the ratio of the top and bottom surface areas of the chimney, allowing the parameter $\tau = \frac{A_t}{A_b}$ to be defined as:
$$\frac{v_b}{v_t} = \tau \tag{3}$$

2. **"Driving potential" $\triangle P$:** Known as the driving potential in a solar chimney, this potential is a "driving" force for airflow from the collector inlet to the top of the chimney, and it essentially measures the pressure difference between the atmospheric pressure at ground level and the static pressure of the hot air stream at the base of the chimney (see Kröger and Blaine (1999) and Tingzhen et al. (2006)):
$$\triangle P = P_0 - P_b. \tag{4}$$
Assuming constant air density and no pressure drop throughout the chimney, the static pressure at the base can be obtained using Bernoulli's equation:
$$P_b + \tfrac{1}{2}\rho v_b^2 + \rho g H_b = \text{const} \quad \Rightarrow \quad \text{const} = P_b + \tfrac{1}{2}\rho v_b^2.$$
Similarly, at the top:
$$\text{const} = P_t + \tfrac{1}{2}\rho v_t^2 + \rho g H_t.$$
Equating constants:
$$P_b + \frac{1}{2}\rho v_b^2 = P_t + \frac{1}{2}\rho v_t^2 + \rho \cdot g \cdot H_t \tag{5}$$
Substituting $P_t = P_0 - \rho_0 g H_{\text{chim}}$ and rearranging yields:
$$\triangle P = (\rho_0 - \rho) \cdot g \cdot H_{chim} + \frac{1}{2}\rho(v_b^2 - v_t^2). \tag{6}$$
Factoring v_b^2 in the difference, we obtain:
$$\Delta P = (\rho_0 - \rho) g H_{\text{chim}} + \tfrac{1}{2}\rho v_b^2 \left(1 - \left(\tfrac{v_t}{v_b}\right)^2\right).$$
Using the continuity equation (3), this can be written in terms of height, base velocity, and the ratio τ:
$$\triangle P = (\rho_0 - \rho) \cdot g \cdot H_{chim} + \frac{1}{2}\rho(v_b^2)(1 - (\tau)^{-2}) \tag{7}$$

This indicates that ΔP increases with higher base velocity and higher τ (for $\tau > 1$), motivating the parametric investigation of τ. Since the Manzanares plant is cylindrical ($\tau = 1$), the second term vanishes, and classically:

$$\triangle P = (\rho_0 - \rho) \cdot g \cdot H_{chim} \tag{8}$$

3. **Parametric study of non-cylindrical chimneys:** A solar chimney is called convergent (cylindrical) if it has zero inclination angle (top left in Fig. 1), and divergent if it has a nonzero angle. The divergence is classified as fully divergent (top right), inlet divergent (bottom right), or outlet divergent (bottom left). When a chimney is divergent ($\tau > 1$), the dynamic pressure at the base has a greater impact, so the pressure difference heavily depends on the base velocity, regardless of the outlet. It is concluded that as τ increases, density and velocity are the variables that most influence the pressure variation, thereby increasing the chimney's efficiency. If the velocity is below 1 m/s, any increase in power is not significant for equation (7), no matter how large τ is; the increase depends on the density ρ, which is small for air. Thus, it is observed that for a solar chimney to be efficient, $v_b > 1$ m/s must be considered, seeking feasible locations. This justifies the focus on localities in the Lambayeque region such as Olmos and Incahuasi, where average wind speeds are about 2.5 m/s and 4.8 m/s, respectively, with minimum values around 1.492 m/s, which, as discussed, allows performing the parametric study of solar chimneys since they exceed 1 m/s. The data were obtained from POWER NASA Project (2024), NASA Langley's Prediction Of Worldwide Energy Resources (POWER) project.

2.6 Selection of configurations and justification of the simulated design

The selection of the 30 solar chimney configurations used in this study is based on scientific precedents that support the use of parametric analyses and computational simulations (CFD) to evaluate the energy performance of these technologies. Haaf's pioneering study, focused on the Manzanares pilot plant, is a key reference as it explored geometric combinations under various environmental conditions through physical and numerical simulations. Subsequent investigations, such as those by Cuce and Murena, also validate this approach, employing between 20 and 50 configurations to characterize the system's behavior, which supports the sample size adopted in this work. Likewise, Xu's study showed that unconventional configurations can achieve notable performance, while Mebarki demonstrated through CFD that geometric simplification can preserve the model's explanatory power regarding the system's thermal behavior. These evidences reinforce the relevance of considering multiple geometric scales as part of the experimental design. Based on these precedents and considering criteria of computational efficiency and representativeness, a set of 30 simulations was defined, structured by 6 scaled geometries combined with 5 levels of solar irradiance. From a statistical perspective, this number of configurations is reasonable for estimating aggregated system parameters, since, under assumptions of independence between simulations and asymptotic normality, the Central Limit Theorem allows approximating the distribution of the system's average performance by a normal distribution, even if the original distribution of the simulated responses is not normal. This property provides an additional basis for comparative analysis and inference on the average behavior of the simulated solar chimneys.

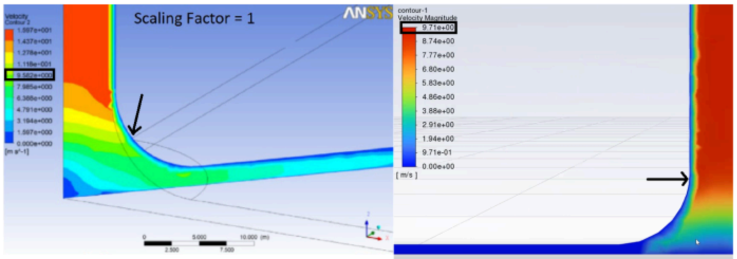

Figure 3: Results obtained from the replicated simulation of the Manzanares experiment for velocity with a scale factor of $C = 1$ and an irradiance of $W = 1000$ W/m^2.

2.7 CFD simulations in Ansys Fluent

In order to better capture small-scale effects independent of length and time scales, the κ-ε turbulence model was chosen. This required configuring the model in Ansys Fluent (whose routines were already implemented, see Menter et al. (2021)). The interaction between air velocity and pressure was examined using the finite volume method for discretization and computation of the unknowns in the continuity, momentum, and energy equations, particularly velocity. For pressure calculation, a second-order one-dimensional Taylor series for Δp was used with a manual adjustment defined as $\Delta p(v) \approx \Delta p(0) + \Delta p'(0)v + \frac{\Delta p''(0)}{2}v^2$, under the boundary conditions of section 2.3, with zero initial values for pressure and its variation with constant acceleration given by $\Delta p(0) = 0$, $\Delta p'(0) = 0$, $\Delta p''(0) = \rho$. These basic assumptions for a solar chimney (Ansys Fluent Inlet) led to the simplified Bernoulli formula $\Delta p = \frac{1}{2}\rho v^2$ used in Murena et al. (2022) (Ansys Fluent Outlet). These manual adjustments were implemented in Ansys Fluent through the "user-defined function" option, setting a convergence criterion of 10^{-6} and working with an air inlet velocity to the collector of 1.3 m/s, based on the good results obtained by that author for the Manzanares simulation.

Finally, after performing simulations at 6 different scales $C = 2^{-n+1}$, with $n \in \{1, \ldots, 6\}$ (see Table 2), a database was generated. It is noted that the results obtained by our simulation (illustratively for velocity, see Fig. 3 right) are quite similar to those obtained by Mebarki et al. (2022). From the extreme values associated with each plot at different scales, data were manually collected for comparison (e.g., 15.97, 11.60, 8.597, 63.03, 46.84, 39.62), data which are not shown in that work (Fig. 4, left-right, top-bottom, respectively). These can be freely seen in Fig. 3 (left) and verified via the database attached to the error plots for velocity and parameters κ and ε (Fig. 5).

2.8 Implementation of the CFD-based methodology using ANSYS Fluent

The data records obtained from a selection of results of various physical variables involved in the simulations carried out in ANSYS Fluent were subsequently processed in the R environment. For this analysis, curvilinear estimation methods were used, considering the parameter *scale* as the independent variable and the velocity values obtained from the simulations at different solar irradiance levels as the dependent variables.

A total of 11 regression models were evaluated: linear, quadratic, cubic, logarithmic, compound, growth, exponential, S-shaped, inverse, and power. For each model, the constants associated with the respective regression equations were estimated, as well as their graphical representation, which allowed a visual and statistical comparison of the fit of the simulated data. In addition, the main statistical indicators for each model were calculated and reported, including coefficient of determination (R^2), the standard error of the estimate, and the ANOVA test, in order to evaluate the overall significance of the fitted model. This analysis made it possible to select the models with the best explanatory capability based on the behavior observed in the numerical simulations.

2.9 Parametric evaluation using Chernoff Faces

In this study, the Chernoff Faces methodology was implemented as a graphical tool to represent multivariate interactions in the design of solar chimneys. This technique allows assigning numerical values of different variables to facial features of a schematic face, thereby facilitating the visual interpretation of complex configurations.

Fifteen facial features were considered, each linked to a different variable, following the coding "RFi" (Facial Feature i). The features used were: face width (RF1), ear height (RF2), upper-face height (RF3), upper-face width (RF4), lower-face width (RF5), nose length (RF6), vertical position of the mouth (RF7), mouth curvature (RF8), mouth length (RF9), eye height (RF10), distance between the eyes (RF11), eye tilt (RF12), pupil eccentricity (RF13), eye diameter (RF14), and pupil position (RF15).

2.10 Association of statistical variables to facial features

Fifteen statistical variables were considered, grouped into three categories: summary variables, variables derived from the analysis of variance (ANOVA), and variables associated with the regression model coefficients. These variables were sequentially assigned to the fifteen facial features (RF1–RF15) defined earlier, respecting a direct correspondence of the form $RFi \leftrightarrow Vi$. This systematic correspondence between statistical variables and visual features enabled generating graphical representations capable of synthesizing the observed multivariate patterns, thus facilitating both the comparison between models and the identification of optimal design profiles for solar chimneys.

The summary variables included the coefficient of determination R^2 (V1) and the standard error of the estimate (V2). The variables related to the analysis of variance were: the sum of squares of regression (V3), the sum of squares of the residual (V4), the degrees of freedom of the regression (V5), the mean square of regression (V6), the F statistic (V7) and its significance level (V8). Finally, among the variables related to the model coefficients were considered: the model constant (V9), the first coefficient of the model (V10), the standardized Beta coefficient (V11), the t-statistic for the constant (V12) and for the variable (V13), and their corresponding significance levels (V14, V15). This systematic assignment allowed generating Chernoff faces where each facial attribute encoded a different statistical aspect of the regression models, enabling intuitive visual comparison.

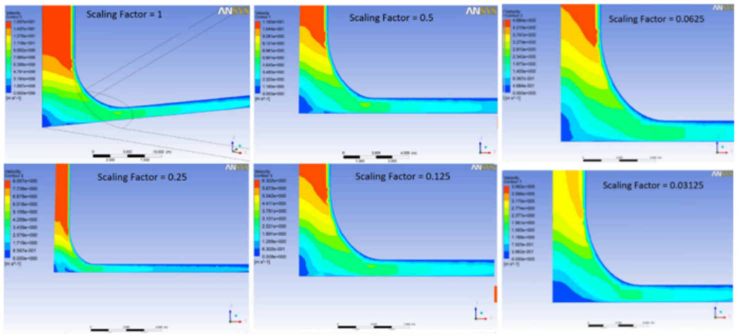

Figure 4: Illustrative graph of the simulation results by Mebarki for velocity across six different scales, used for the collection of extreme values for comparison purposes.

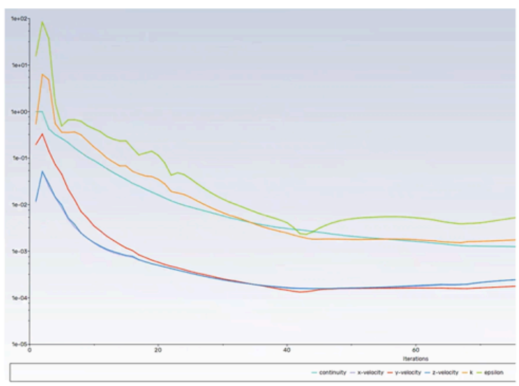

Figure 5: Error plot for the velocity variable and turbulence parameters κ and ε, derived from the replicated CFD simulation of the Manzanares experiment at $C = 1$ and $W = 1000$ W/m^2.

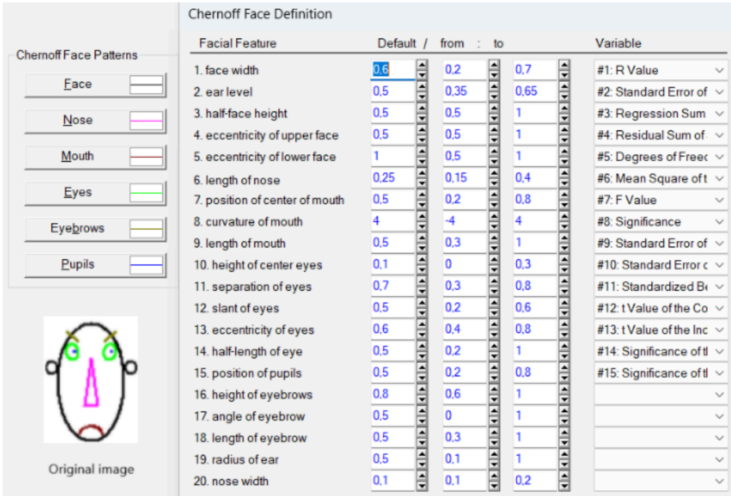

Figure 6: Facial attributes of Chernoff Faces mapped with statistical analysis variables for regression model selection in the parametric study of solar chimneys.

3. RESULTS

3.1 Regression results obtained in R

The statistical results derived from the numerical simulations performed in ANSYS Fluent were processed in the R environment, applying curvilinear fitting with a tolerance of 0.0001. Eleven regression models were evaluated, with the axial velocity (v_z), referred to in this study as V_m, selected as the dependent variable, and the system's geometric scale as the independent variable. For each model, adjusted equations were generated and relevant values from three statistical blocks were extracted: the model summary, the ANOVA table, and the model coefficients. Four models (inverse, quadratic, cubic, and power) were selected as representative to be subsequently compared using Chernoff face visualizations, the results of which are detailed in Tables 2 through 5. Finally, the data from the 11 models were summarized in a table structured with 15 statistical variables per model (Table 6), used as the basis for constructing the faces in the multivariate visual analysis. Although consistent results were obtained for other simulated variables such as pressure, mass flow, and temperature, only those corresponding to V_m are reported, as it is the most relevant variable according to the literature review.

Table 2: Statistical results of the inverse regression model obtained in R

Model Summary				
R	R^2	**Adjusted** R^2	**Std. Error of Estimate**	
0.794	0.630	0.538	2.331	
ANOVA				
Source	**Sum of Squares**	**df**	**Mean Square**	**F / Sig.**
Regression	37.039	1	37.039	6.819 / 0.059
Residual	21.728	4	5.432	–
Total	58.767	5	–	–
Coefficients				
Variable	**Coefficient (B)**	**Std. Error**	**Beta**	**t / Sig.**
$1/\text{scale}$	-0.229	0.088	-0.794	-2.611 / 0.059
Constant	8.235	1.325	–	6.214 / 0.003

Table 3: Statistical results of the quadratic regression model obtained in R

Model Summary				
R	R^2	**Adjusted** R^2	**Std. Error of Estimate**	
0.997	0.995	0.991	0.320	
ANOVA				
Source	**Sum of Squares**	**df**	**Mean Square**	**F / Sig.**
Regression	58.459	2	29.230	284.912 / 0.000
Residual	0.308	3	0.103	–
Total	58.767	5	–	–
Coefficients				
Variable	**Coefficient (B)**	**Std. Error**	**Beta**	**t / Sig.**
x^2	-7.081	1.492	-0.811	-4.748 / 0.018
x	16.312	1.580	1.764	10.326 / 0.002
Constant	2.047	0.250	–	8.190 / 0.004

Table 4: Statistical results of the cubic regression model obtained in R

Model Summary				
R	R^2	**Adjusted R^2**	**Std. Error of Estimate**	
1.000	0.999	0.998	0.135	
ANOVA				
Source	**Sum of Squares**	**df**	**Mean Square**	**F / Sig.**
Regression	58.730	3	19.577	1072.970 / 0.001
Residual	0.036	2	0.018	–
Total	58.767	5	–	–
Coefficients				
Variable	**Coefficient (B)**	**Std. Error**	**Beta**	**t / Sig.**
x^3	14.886	3.860	1.735	3.856 / 0.061
x^2	-29.069	5.737	-3.329	-5.067 / 0.037
x	23.903	2.078	2.584	11.501 / 0.007
Constant	1.606	0.156	–	10.320 / 0.009

Table 5: Statistical results of the power regression model obtained in R

Model Summary				
R	R^2	**Adjusted R^2**	**Std. Error of Estimate**	
1.000	1.000	1.000	0.000	
ANOVA				
Source	**Sum of Squares**	**df**	**Mean Square**	**F / Sig.**
Regression	1.858	1	1.858	1.003×10^{11} / < 0.001
Residual	0.000	4	0.000	–
Total	1.858	5	–	–
Coefficients				
Variable	**Coefficient (B)**	**Std. Error**	**Beta**	**t / Sig.**
$\ln(\text{scale})$	0.470	0.000	1.000	316760.990 / < 0.001
Constant	11.324	0.000	–	321078.645 / < 0.001

Table 6: Dataset of 11 regression models with 15 selected statistical measures for the chosen variable (velocity V_m)

Model	R	Std. Error	Reg SS	Res SS	Reg df	Reg MS	F	Sig	Std. Error (Const)	Std. Error (Var)	Beta	t (Const)	t (Var)	Sig (Const)	Sig (Var)
Linear	0.981	0.985	101.522	3.883	1.000	101.522	104.590	0.001	0.560	1.189	0.981	8.086	10.227	0.001	0.001
Logarithmic	0.967	1.303	98.611	6.793	1.000	98.611	58.063	0.002	0.943	0.449	0.967	15.324	7.620	0.002	0.002
Quadratic	0.997	0.320	98.311	0.456	2.000	49.155	477.632	¡0.001	0.163	0.333	0.997	20.011	13.169	¡0.001	0.001
Cubic	1.000	0.135	58.230	0.036	3.000	19.410	1070.00	0.001	0.156	0.271	0.998	10.320	11.501	0.009	0.007
Exponential	0.975	0.070	98.217	26.495	1.000	98.217	75.574	0.001	0.726	0.296	0.975	12.107	8.392	0.001	0.004
Power	1.000	0.000	1.858	0.000	1.000	1.858	1.003×10^{11}	¡0.001	0.000	0.000	1.000	316760.99	321078.65	¡0.001	¡0.001
Inverse	0.794	2.331	37.039	21.728	1.000	37.039	6.819	0.059	0.088	1.325	0.794	-2.611	6.214	0.059	0.003
Logistic	0.987	0.551	69.331	4.542	2.000	34.666	54.394	¡0.001	0.268	0.874	0.987	14.849	7.968	¡0.001	0.012
S-Curve	0.991	0.407	58.366	1.853	2.000	29.183	180.31	¡0.001	0.365	0.392	0.991	10.094	7.441	0.001	0.012
Growth	0.959	0.942	86.466	11.529	1.000	86.466	91.792	0.000	0.782	2.212	0.959	11.787	8.805	0.002	0.008
Compound	0.966	0.802	82.105	5.034	1.000	82.105	102.323	¡0.001	0.593	1.201	0.966	11.256	9.229	0.002	0.000

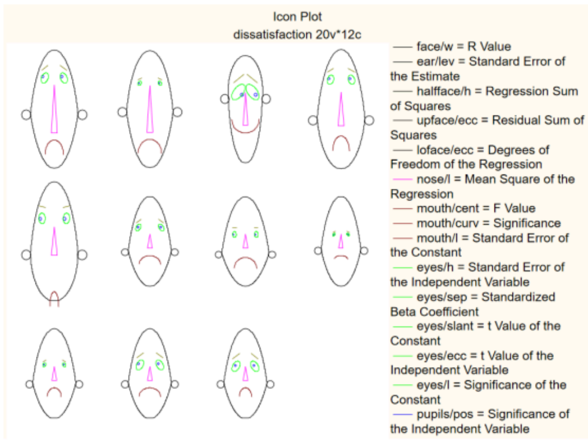

Figure 7: Chernoff Faces for the 11 regression models in Scenario 1: expression of dissatisfaction.

3.2 Model selection using Chernoff Faces

A visual analysis using Chernoff Faces was applied to identify the most suitable nonlinear regression model among eleven candidates: linear (C1), logarithmic (C2), inverse (C3), quadratic (C4), cubic (C5), compound (C6), power (C7), S-curve (C8), growth (C9), exponential (C10), and logistic (C11). The selection was based on the highest correlation coefficient values (R) and the generated facial representation, which allowed discarding eight models and focusing the evaluation on the three most promising ones.

3.3 Validation and permutation of variables

To address potential biases in the visual representation, permutations were performed in the assignment of variables to facial features, analyzing three scenarios: default configuration (Figure 7), features expressing overconfidence (Figure 8), and features reflecting emotional stability (Figure 9). The final selection was based on the intersection of the "best faces" across the three contexts.

The criteria considered included error deviation, sum of squares (regression and residual), degrees of freedom, mean square, F-value and its significance, as well as standard errors and t-values for both the constant and the independent variable, standardized Beta coefficient, and associated significance levels.

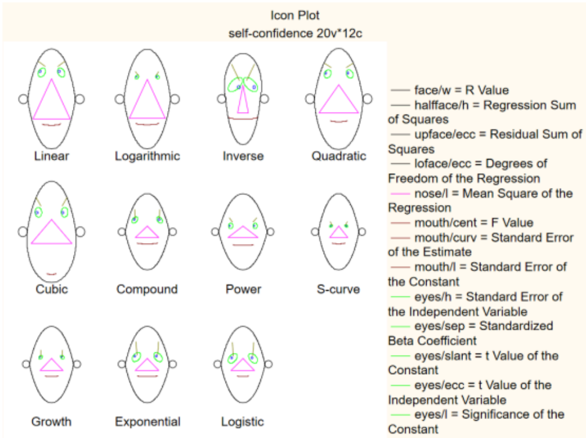

Figure 8: Chernoff Faces for the 11 regression models in Scenario 2: expression of self-confidence.

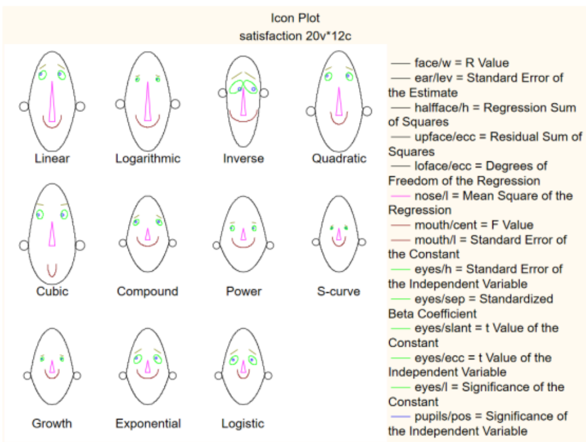

Figure 9: Chernoff Faces for the 11 regression models in Scenario 3: expression of satisfaction.

Based on this cross-evaluation, it was concluded that the most robust and consistent regression model was the **power model**, represented in Figure 10, as it displayed the most favorable facial features across the three visual scenarios considered.

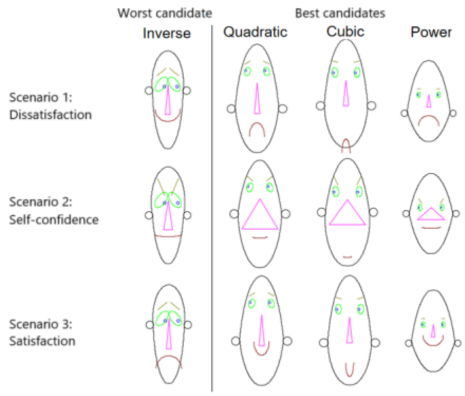

Figure 10: Chernoff Faces: the power model as the strongest candidate across all three scenarios.

3.4 Statistical confirmation of the selected model

Table 7 presents the coefficients estimated in R for the power regression model, which achieved a perfect fit on the simulated data. The final equation for air velocity (V_m), as a function of the geometric scale (C), was defined as:

$$V_m = 14.177 \cdot C^{0.416} \quad \text{(m/s)}$$

This expression matches very closely the one proposed by Mebarki et al. (2022), who obtained for an irradiance of 1000 W/m^2 the equation $V_m = 14.17 \cdot C^{0.415}$, reinforcing the validity and replicability of the present model.

Table 7: Estimated coefficients in R for the power regression model

Variable	B	Std. Error	Beta	t / Sig.	
Constant	14.177	0.000	1.000	273733.089	<0.001
$\ln(C)$	0.416	0.000	1.000	238800.033	<0.001

3.5 Independence from chosen scenarios in model selection

To confirm that the choice of model was not solely dependent on the proposed visual scenarios, the database was standardized and a new analysis using Chernoff Faces was performed. This new scenario focused on faces representative of "statistical normality" (friendly appearance), as shown in Figure 11. In this context, the most favorable models were the fifth (cubic) and the seventh (power), although the fourth (quadratic) could also be considered acceptable.

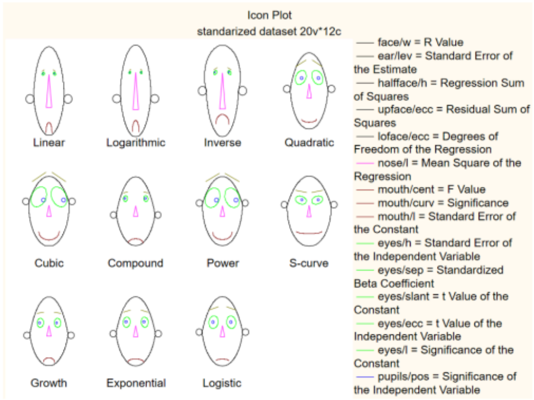

Figure 11: Chernoff Faces: confirmatory analysis with standardized dataset.

Given the visual similarity between the faces corresponding to models 5 and 7, both were individually analyzed without standardization. Considering that the most influential variables in a regression model are usually significance and R value, a permutation was performed excluding both variables to observe the impact of the remaining parameters. This strategy is supported by Chrobak et al. (2017), who suggests that "when only a few variables are considered, particular attention must be paid to which facial features are changing." In Figure 12, it is evident that even without considering these two key variables, model 7 (power) continues to present the most balanced face, confirming its robustness as the selected model.

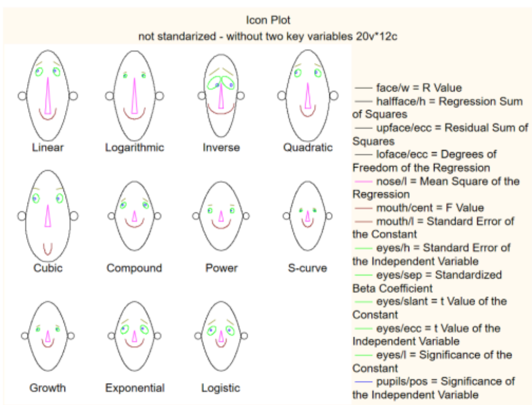

Figure 12: Chernoff Faces: second confirmatory analysis without standardization or key variables.

3.6 Validation of selected model by Chernoff faces

A normality test was applied to the differences between the predictions of the cubic and power models. The Shapiro-Wilk normality test yielded a value of $W = 0.851$ with $p = 0.162$, indicating that the differences follow a normal distribution. The paired sample Pearson correlation was extremely high ($r = 0.9999$, $p < 0.001$), indicating an almost perfect correspondence in the prediction patterns without implying exact collinearity. A paired samples t-test yielded $t = -1.147$ (reported as $|t| = 1.147$) with $p = 0.303$, indicating that there are no statistically significant differences between the means of the two models. Together, these results support the statement that both models are statistically equivalent in predictive capacity. However, the power model was chosen for its greater functional simplicity, its theoretical coherence with the physical behavior of the phenomenon, and its more balanced visual representation according to the Chernoff faces methodology.

Table 8: Summary of normality, correlation, and paired t-test for the cubic and power models with respect to the velocity variable at 1000 W/m^2 irradiance

Test	Statistic	Sig. (p)
Shapiro-Wilk normality test	0.851	0.162
Paired sample Pearson correlation (r)	0.9999	<0.001
Paired t-test (Student's t)	1.147	0.303

3.7 Theoretico-experimental validation

The validity of the obtained power regression model is reinforced by comparing it with the equation reported by Mebarki et al. (2022), who, using experimental data from the Manzanares solar plant, proposed a similarly structured model for the air velocity variable. However, that study does not detail the methodological criteria or statistical basis that justify the selection of their model. In contrast, the present study has incorporated a combined theoretical-statistical approach that rigorously grounds the selection of the most appropriate regression model.

3.8 CFD equations with statistical justification

As a result of the statistical analysis of the simulated data under different irradiance conditions, the power regression equation was found to best represent the behavior of the air velocity variable (V_m) as a function of the scale parameter (C) in a solar chimney. The expressions found for five different irradiance levels (W) are stated below:

$$\begin{cases} V_m = 14.17 \cdot C^{0.415}, & W = 1000\ \text{W/m}^2 \\ V_m = 13.45 \cdot C^{0.417}, & W = 800\ \text{W/m}^2 \\ V_m = 12.87 \cdot C^{0.429}, & W = 600\ \text{W/m}^2 \\ V_m = 12.24 \cdot C^{0.448}, & W = 400\ \text{W/m}^2 \\ V_m = 11.32 \cdot C^{0.470}, & W = 200\ \text{W/m}^2 \end{cases} \tag{9}$$

These expressions are not only consistent with the physical principles governing fluid dynamics in solar chimneys, but have also been validated through both statistical and visual contrast using Chernoff Faces.

3.9 Graphical comparison of models

To reinforce the previous findings, a graphical comparison is presented of the velocity curves obtained from the power regression for different irradiance levels. Figure 13 shows the results generated using R, accurately replicating the characteristics reported in the literature. Meanwhile, Figure 14 displays the original results obtained by Mebarki et al. (2022).

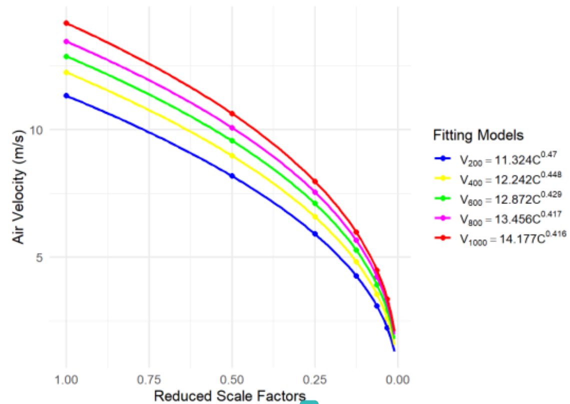

Figure 13: Results replicated using power regression: Air velocity (V_m) as a function of scale factors (C), under five different solar irradiance levels.

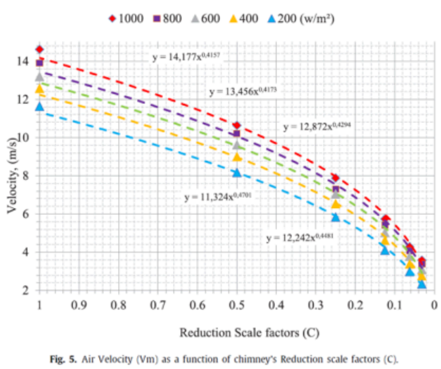

Figure 14: CFD results from Mebarki et al. (2022): Air velocity (V_m) as a function of scale (C), at six irradiance levels.

3.10 Efficiency and performance results

Based on the velocity values obtained in the previous section, the power output of the system was calculated using the mathematical models developed in section 1.3. Using experimental data from Xu and Zhou (2018), a mass flow of $\dot{m} = 987.50$ kg/s (according to MFR in Table 5) and an air density of $\rho = 1.103$ kg/m^3 (according to Table 3) were considered, which allows calculating the volumetric flow as:

$$V = \frac{\dot{m}}{\rho} = \frac{987.50\ \text{kg/s}}{1.103\ \text{kg/m}^3} \approx 895.29\ \text{m}^3/\text{s} \tag{10}$$

For the calculation of power output under different conditions, the following configurations were used:

- **Using the geometric efficiency parameter** χ (Eq. 1): The turbine efficiency was taken as $\eta_{\text{turb}} = 0.83$ (see Haaf et al. (1983), p. 153), $\chi = 2/3$ (Table 3 in Cuce et al. (2020)), $\Delta p_{\text{poten}} = 68.32$ Pa (TPP according to Xu and Zhou (2018)), and V obtained above. The resulting calculation is:

  $$P = 0.83 \cdot \left(\frac{2}{3}\right) \sqrt{1 - \left(\frac{2}{3}\right)} \cdot 68.32 \cdot 895.29 \approx 19.5\ \text{kW}.$$

  This value matches that reported in Table 5 of Xu and Zhou (2018), confirming the consistency between the proposed model and the simulated data.

- **Without considering the parameter** χ (Eq. 2): $\Delta p_{\text{turb}} = 82.9$ Pa (Table 3 in Xu and Zhou (2018)) was used and $V = 574.07$ m^3/s. The power was obtained as:

  $$P = 0.83 \cdot 82.9 \cdot 574.07 \approx 39.5\ \text{kW}.$$

  This result approximates the ideal experimental power (40 kW) and improves the experimentally recorded value at the Manzanares plant (36 kW) according to Haaf et al. (1983), demonstrating the effect of the parameter χ on the overall system efficiency.

3.11 Summary of Results

1. The usefulness of the Chernoff Faces approach was confirmed as a complementary tool in multivariate analysis, allowing for the structured and visual interpretation of complex mathematical models.

2. For the key variable in this study, air velocity (V_m), it was observed that—regardless of the irradiance level—the inverse regression model consistently performed the worst. In contrast, the quadratic, cubic, and power models demonstrated superior predictive fit, as illustrated in Figures 3, 4, and 5, respectively.

3. The findings demonstrate that integrating Chernoff Faces with traditional statistical and simulation tools constitutes an innovative and effective methodological strategy for the evaluation, validation, and optimization of solar systems.

4. DISCUSSION

4.1 Comparison of results

Results from the original paper Xu and Zhou (2018):

1. Velocity, pressure difference, mass flow, efficiency, and electric power decrease as the scale factors (C) are reduced.

2. Empirical equations were proposed to model the changes in variables such as air velocity, pressure, temperature, mass flow, and electric power as functions of different reduced scale factors relative to a reference solar plant.

Results of the present study:

1. It is confirmed that performance systematically decreases with scale reduction, in agreement with previous findings.

2. Unlike previous work, a robust statistical basis is provided that justifies the selection of regression models —especially power-type— to model air velocity, pressure, temperature, mass flow, and electric power as functions of the scale parameter.

4.2 General summary of findings

The present work expanded the classic approach by incorporating multivariate and visual analysis with Chernoff faces, as well as statistical validation through permutations and contrasts. In particular, three different visual configurations and multiple statistical scenarios were analyzed to evaluate the robustness of the selected model. The power regression model was identified as the most suitable, not only for its numerical fit but also for its visual coherence, simplicity, and theoretical support in the literature.

In addition, key geometric variables that had not been addressed in depth in previous research were integrated, such as the height of the chimney, its radius, and the dimensions of the collector. This made it possible to understand more clearly how geometric variations affect the overall performance of the system.

4.3 Discussion on the added value of the visual approach

The use of Chernoff faces allowed graphically representing 15 performance and design variables in a single schematic face. This approach facilitated comparison between regression models and intuitively revealed complex patterns that could go unnoticed in purely numerical analyses. The inclusion of permutations and variable standardization showed that the technique is robust against configuration changes and allows the selection of models without visual biases.

When observing the generated facial configurations, it was found that scale reduction systematically worsens the visual performance of the system, highlighting the design's sensitivity to this parameter. This visualization corroborated the quantitative findings and reinforced the methodological decision to integrate graphical tools with inferential statistics.

4.4 Implications of the study

The obtained results not only provide a robust model for simulating the behavior of solar chimneys under different scales and irradiance levels, but also introduce a replicable methodological approach for visualization-assisted design. This type of tool can be key to optimizing prototypes, evaluating design alternatives, and reducing modeling errors in the preliminary stage of solar engineering projects.

5. CONCLUSIONS

1. Mathematical models from relevant research were analyzed and the results obtained from computational simulations based on partial differential equations in the CFD field were replicated using a rigorous statistical approach. This procedure improved the understanding of the key factors that influence the performance and efficiency of solar chimneys.

2. Unlike more reductionist approaches, this study addressed in a broad and well-founded way the selection of the most appropriate model, considering not only classic metrics such as the coefficient of determination (R^2) and validation via the t-test, but also integrating multivariate graphical tools. The results demonstrate that the use of Chernoff faces is a robust visual and analytical tool for the evaluation and optimization of solar systems.

3. The application of Chernoff faces proved to be highly effective and intuitive for the analysis of multidimensional data in solar engineering. This technique allowed visually identifying significant interactions between variables, strengthening decision-making in the design of solar chimneys. Likewise, the approach proposed here opens new possibilities for incorporating advanced visualization techniques in engineering and scientific contexts.

4. In line with Hananel et al. (2023), it is confirmed that analysis using Chernoff faces is not a trivial technique but a powerful methodology for revealing complex patterns through multivariate visualization. By showing that it is more effective to condense multiple variables in terms of visual synthesis (instead of fragmented analyses), it is concluded that this tool can serve as a methodological bridge between descriptive analysis and interpretive synthesis. This methodological shift represents an intellectual challenge of greater depth, aligned with the demands of advanced research.

ACKNOWLEDGMENTS

The authors thank the Department of Mathematical Analysis of the University of Granada for the support provided during the development of international activities related to this research. They also express their gratitude to the Santo Toribio de Mogrovejo Catholic University (USAT) for the funding granted under the 2025 Research Projects Competition, which enabled the acquisition of the software necessary for the development of this article.

DATA AVAILABILITY STATEMENT

The datasets generated and/or analyzed during the current study are not publicly available, but they may be obtained from the corresponding author upon reasonable request.

REFERENCES

Chernoff, H., The use of faces to represent points in k-dimensional space graphically, *Journal of the American Statistical Association*, vol. **68**, no. 342, pp. 361–368, 1973.
URL https://www.tandfonline.com/doi/abs/10.1080/01621459.1973.10482434

Chrobak, R., Sempere, P.G., Prieto, A.B., and Avalos, K.R., Exploración sobre las estrategias de enseñanza de docentes de ingeniería para para el logro de habilidades creativas e innovadoras en sus estudiantes, 2017.

Cuce, E., Sen, H., and Cuce, P.M., Numerical performance modelling of solar chimney power plants: Influence of chimney height for a pilot plant in manzanares, spain, *Sustainable Energy Technologies and Assessments*, vol. **39**, p. 100704, 2020.

Cuicas Ávila, M., Debel Chourio, E., Casadei Carniel, L., and Álvarez Vargas, Z., El software matemático como herramienta para el desarrollo de habilidades del pensamiento y mejoramiento del aprendizaje de las matemáticas, *Actualidades investigativas en educación*, vol. **7**, no. 2, pp. 1–34, 2007.

F Medina Martínez, N., Las variables complejas en investigaciones pedagógicas, 2017.

Flury, B. and Riedwyl, H., Graphical representation of multivariate data by means of asymmetrical faces, *Journal of the American Statistical Association*, vol. **76**, no. 376, pp. 757–765, 1981.

Haaf, W., Friedrich, K., Mayr, G., and Schlaich, J., Solar chimneys part i: principle and construction of the pilot plant in manzanares, *International Journal of solar energy*, vol. **2**, no. 1, pp. 3–20, 1983.

Hananel, A., Loaiza, S., and Collantes, J., An analysis of final grades in a mathematics course for the enhancement of upcoming engineering students' academic performance by using multivariate statistical techniques, Vol. 3691, pp. 114–129, 2023.

Hu, S., Leung, D.Y., and Chan, J.C., Numerical modelling and comparison of the performance of diffuser-type solar chimneys for power generation, *Applied Energy*, vol. **204**, pp. 948–957, 2017.

Kröger, D. and Blaine, D., Analysis of the driving potential of a solar chimney power plant, *South African Inst. of Mechanical Eng. R & D J*, vol. **15**, pp. 85–94, 1999.

Mebarki, A., Sekhri, A., Assassi, A., Hanafi, A., and Marir, B., CFD analysis of solar chimney power plant: Finding a relationship between model minimization and its performance for use in urban areas, *Energy Reports*, vol. **8**, pp. 500–513, 2022.

Menter, F., Sechner, R., and Matyushenko, A., Best practice: Rans turbulence modeling in ansys cfd, *ANSYS Inc.: Canonsburg, PA, USA*, 2021.

Murena, F., Gaggiano, I., and Mele, B., Fluid dynamic performances of a solar chimney plant: Analysis of experimental data and CFD modelling, *Energy*, vol. **249**, no. C, 2022.

Olmos, E., El rendimiento estudiantil: una metodología para su medición, *Revista Economía*, vol. **13**, pp. 7–26, 1997.

POWER NASA Project, The prediction of worldwide energy resource (power), https://power.larc.nasa.gov/, , 2024, nASA Applied Sciences Program within the Earth Science Division of the Science Mission Directorate.

Santos, A.R.P. and Peña, O.F.C., ¿ Qué piensan los estudiantes universitarios frente a la formación investigativa?, *REDU. Revista de Docencia Universitaria*, vol. **15**, no. 2, pp. 57–76, 2017.

Tingzhen, M., Wei, L., and Guoliang, X., Analytical and numerical investigation of the solar chimney power plant systems, *International Journal of Energy Research*, vol. **30**, no. 11, pp. 861–873, 2006.

Velazco Lorenzo, D. and Butler Blacker, J.G., Desarrollo de un modelo experimental de una chimenea solar-eólica para suministro eléctrico, *TECNIA*, vol. **32**, no. 1, pp. 13–27, 2022.

Xu, Y. and Zhou, X., Performance of divergent-chimney solar power plants, *Solar Energy*, vol. **170**, pp. 379–387, 2018.

articulo_upeu_2 (21) (1).pdf

INFORME DE ORIGINALIDAD

7%	4%	6%	1%
INDICE DE SIMILITUD	FUENTES DE INTERNET	PUBLICACIONES	TRABAJOS DEL ESTUDIANTE

FUENTES PRIMARIAS

1	Proceedings of ISES World Congress 2007 (Vol I – Vol V), 2009. Publicación	1%
2	e-sciencecentral.org Fuente de Internet	<1%
3	Submitted to University College London Trabajo del estudiante	<1%
4	Ammar Mebarki, Adel Sekhri, Abdelhalim Assassi, Abdelhakim Hanafi, Belkacem Marir. "CFD analysis of solar chimney power plant: Finding a relationship between model minimization and its performance for use in urban areas", Energy Reports, 2022 Publicación	<1%
5	"Cold Inflow-Free Solar Chimney", Springer Science and Business Media LLC, 2021 Publicación	<1%
6	pmc.ncbi.nlm.nih.gov Fuente de Internet	<1%
7	c.coek.info Fuente de Internet	<1%
8	ceur-ws.org Fuente de Internet	<1%
9	penerbit.uthm.edu.my Fuente de Internet	<1%

10	www.witpress.com Fuente de Internet	<1 %
11	"Chapter 550 Flow Measurement", Springer Science and Business Media LLC, 2008 Publicación	<1 %
12	ijibm.site666.com Fuente de Internet	<1 %
13	Morteza Bayareh. "Exergy analysis of solar chimney power plants: A review", Sustainable Energy Technologies and Assessments, 2022 Publicación	<1 %
14	Saeed Bagheri, Madjid Ghodsi Hassanabad. "Numerical and experimental investigation of a novel vertical solar chimney power plant for renewable energy production in urban areas", Sustainable Cities and Society, 2023 Publicación	<1 %
15	nanopdf.com Fuente de Internet	<1 %
16	sutir.sut.ac.th:8080 Fuente de Internet	<1 %
17	Tenko Raykov. "Chapter 90 Canonical Correlation Analysis", Springer Science and Business Media LLC, 2025 Publicación	<1 %
18	Víctor Miñambres-Marcos, Enrique Romero-Cadaval, Miguel A. Guerrero-Martínez, María Isabel Milanés-Montero. "Cooperative operation of inverters for grid-connected photovoltaic generation systems", Electric Power Systems Research, 2013 Publicación	<1 %

19	Rizgar Bakr Weli, Soorkeu A. Atrooshi, Ruediger Schwarze. "Investigation of the performance parameters of a sloped collector solar chimney model – An adaptation for the North of Iraq", Renewable Energy, 2021 Publicación	<1 %
20	Viviana Sarmiento, Kristin Hamre, Aleksander Arnø, Joshua Dagogo, Elisabeth Ødegård, Odd Elvebø, Pedro Araujo. "Stability study and validation of a liquid chromatography tandem mass spectrometry method for the quantitative analysis of polyphenols in fish feed ingredients", Journal of Chromatography B, 2024 Publicación	<1 %
21	www.hindawi.com Fuente de Internet	<1 %
22	www.mdpi.com Fuente de Internet	<1 %
23	www.researchgate.net Fuente de Internet	<1 %
24	www.sciencepublishinggroup.com Fuente de Internet	<1 %
25	Md. Ezaz Ahammed, Ajay Kumar Yadav, T. Laxminidhi. "Numerical study on temperature distribution during magnetic hyperthermia of different tumor tissues", Journal of Magnetism and Magnetic Materials, 2024 Publicación	<1 %
26	Mohamed S. Shahin, Mehmet F. Orhan, Kenan Saka, Ahmed T. Hamada, Faruk Uygul. "Energy Assessment of an Integrated Hydrogen	<1 %

Production System", International Journal of Thermofluids, 2022
Publicación

27 Safer Nabil Belkacem. "Effects of Ambient Temperature and Solar Radiation on Solar Chimney Power Plants (SCPP) Performances", International Review of Mechanical Engineering (IREME), 2022 <1 %
Publicación

28 doi.org <1 %
Fuente de Internet

29 link.springer.com <1 %
Fuente de Internet

30 www.cell.com <1 %
Fuente de Internet

31 Erdem Cuce, Pinar Mert Cuce, Harun Sen. "A thorough performance assessment of solar chimney power plants: Case study for Manzanares", Cleaner Engineering and Technology, 2020 <1 %
Publicación

32 Mohammad Mahdi Esmaili, Seyyed Hossein Fallah, Morteza Izanlu, Mohammad Sadegh Valipour. "Investigation on the Performance of a solar chimney-flare gas hybrid system", Sustainable Energy Technologies and Assessments, 2022 <1 %
Publicación

33 Shuoshuo Xu, Jinxing Lai, Brendan C. O’Kelly, Budi Zhao. "Characterizing internal flow mechanisms in reverse extrusion tests using X-ray CT and marker tracking", Acta Geotechnica, 2025 <1 %

Publicación

34	docslib.org Fuente de Internet	<1 %
35	dokumen.pub Fuente de Internet	<1 %
36	openaccess.city.ac.uk Fuente de Internet	<1 %
37	www.frontiersin.org Fuente de Internet	<1 %
38	www.wjoud.com Fuente de Internet	<1 %
39	zealpress.com Fuente de Internet	<1 %
40	Erdem Cuce, Pinar Mert Cuce, Salvatore Carlucci, Harun Sen, Kumarasamy Sudhakar, Md. Hasanuzzaman, Reza Daneshazarian. "Solar Chimney Power Plants: A Review of the Concepts, Designs and Performances", Sustainability, 2022 Publicación	<1 %
41	Fanlong Meng, Andreas Gross, Hermann F. Fasel. "Computational Fluid Dynamics Investigation of Solar Chimney Power Plant", 43rd Fluid Dynamics Conference, 2013 Publicación	<1 %
42	Ghassan F. Smaisim, Azher M. Abed, Ali Shamel. "Modeling the Thermal Performance for Different Types of Solar Chimney Power Plants", Complexity, 2022 Publicación	<1 %

43 Siyang Hu, Dennis Y.C. Leung, John C.Y. Chan. "Numerical modelling and comparison of the performance of diffuser-type solar chimneys for power generation", Applied Energy, 2017 <1%

Publicación

Excluir citas	Activo	Excluir coincidencias	< 5 words
Excluir bibliografía	Activo		